APPLICATION OF A LOCALLY-COUPLED NUMERICAL METHOD TO BUOYANT SWIRLING FLOW IN A VERTICAL CILINDRICAL CHAMBER

Marcelo J.S. de Lemos
Departamento de Energia - IEME
Instituto Tecnológico de Aeronáutica - ITA
12228-900, São José dos Campos, SP, Brasil. E-mail: *delemos@mec.ita.br*

Abstract

This work reports numerical results for the case of incompressible laminar heated flow with a swirl in a vertical cylindrical chamber. Computations are obtained with a point-wise block-implicit scheme. Flow governing equations are written in terms of the so-called primitive variables and are recast into a general form. The discretized momentum equations are applied to each cell face and then, together with the mass-continuity, tangential velocity and energy equations, are solved directly in each computational node. The effects of Rayleigh, Reynolds and Swirl numbers on the temperature field are discussed upon. Flow pattern and scalar residual history are reported. Further, it is expected that more advanced parallel computer architectures can benefit from the error smoothing operator here described.

Keywords: Model Furnace, Numerical Methods, Implicit Solution, Coupled Solution, Buoyancy

1. INTRODUCTION

Today, new technologies for efficient energy production are based on the so-called lean and low-NOx combustion. Accordingly, an ascending stream with an induced swirling motion characterizes most flow fields in such systems. Swirling induces flame stabilization allowing peak temperature reduction, ultimately reducing pollutant formation rates.

In such cases, the buoyancy term together with the centripetal and Coriollis accelerations make the system of governing equations of a high degree of coupling. Linearization of governing equations followed by the use of iterative solvers is the common route found in the literature for solving such nonlinear problems.

Segregated methods, in which one individual flow variable is relaxed while holding the others still, are known to be rather sensitive when handling strong physical coupling. For that, the so-called *coupled* solvers, where all dependent variables are relaxed in the same domain location, have received much attention lately.

For buoyancy-driven laminar flows, benchmark solutions for the field in a square cavity have been presented [1]. Multi-grid solution for this problem has also been published [2]. In the great majority of those works a segregated method is generally employed with the repetitive solution of a pressure or pressure-correction equation, followed by subsequent updates of the velocity and scalar fields. This strategy forms the basis of the SIMPLE family of algorithms [3]. Coupled line solvers for the temperature and velocity fields have shown improvements in computer time requirements for natural convection flows with large Rayleigh numbers [4]. The work in [4] is an indication of the advantage of coupled schemes for solving algebraic equations set with a high degree of interlinkage among the variables. Recently, the block implicit technique has also been applied to calculation of buoyant flows in a partially-coupled manner [5].

For swirling flows, most solutions found in the literature are also based on segregated relaxation procedures [6-8]. In the present context, a fully-implicit treatment is associated with the idea of simultaneously updating flow and scalar fields at each step within the error smoothing operator. To the best of the author's knowledge, in all published work, neither temperature nor tangential velocity fields, seen here as *scalars*, are treated in a fully implicit manner.

Following the aforementioned and based on Vanka's SGCS method [9, 10], simulated lid-driven cavity fluid motion through a cylindrical tank using a block-implicit numerical scheme was presented in [11]. Later, the technique was extended to buoyancy-driven streams [12], including vertical [13] and inclined cavities [14] in addition to calculation of swirling flows in model combustor [15]. In those papers, a fully-implicit treatment for the scalar (temperature or tangential velocity) was made use of.

The objective of this paper is to further extend the technique presented in [12, 13] for temperature and in [15] for the azimuthal velocity, combining now the solution of both scalars into a single fully-implicit numerical treatment. To this end, computations are presented for a model furnace comprising incompressible laminar flow simultaneously heated and subjected to an incoming flow with swirl. Effects of Reynolds, Rayleigh number and swirling strength on temperature patterns and convergence rates are reported.

2. GOVERNING EQUATIONS AND NUMERICAL METHOD

Geometry. The geometry here considered is schematically shown in Figure 1. A typical furnace combustion zone is approximated by a model consisting of a circular chamber of constant radius R and height H. At inlet, the mixture air+fuel enters through a circular slot of clearance r_1-r_2. At one diameter downstream the entrance, combustion gases are able to exit through an annulus of thickness r_3-r_4. The temperature level is prescribed over the entire lateral wall and on the bottom and top lids, except at the exit area where a null temperature gradient is assumed to be established by the outward motion of the fluid.

Although it is recognized that the geometry of Figure 1 might be an oversimplification of state-of-the-art industrial furnaces, essential elements, namely *swirl*, *buoyancy* and *recirculating zones* provide a good test case for the numerical method here discussed.

Compact notation. The conservation equations for mass, momentum and energy here analyzed can be written in a compact form if the existing analogies among the processes of accumulation, transport, convection and generation/destruction of those quantities are observed. This generic equation is commonly known in the literature as the *general transport equation* and can be written in its conservative two-dimensional laminar for *axi-symmetric* cases as:

$$\frac{\partial}{\partial z}\left[\rho W \phi - \Gamma_\phi \frac{\partial \phi}{\partial z}\right] + \frac{1}{r}\frac{\partial}{\partial r}\left[r\left(\rho U \phi - \Gamma_\phi \frac{\partial \phi}{\partial r}\right)\right] = S_\phi \quad \textbf{(1)}$$

In equation (1) ϕ can represent any quantity of vectorial or scalar nature (velocity or temperature), ρ is the fluid density, U and W are the velocity components in the r- and z-directions, respectively, Γ_ϕ is the transport coefficient for diffusion and S_ϕ is the source term. Table 1 identifies correspondent terms for the different equations represented by (1). In both Table 1 and equation (1) gravity acts in the z-direction, μ is the fluid viscosity, Pr the Prandtl number, T the temperature and V the tangential velocity component.

Computational grid and finite-difference formulation. In this work, the set of equations for mass, momentum and energy above is *differentiated* by means of the widely-used control-volume approach of Patankar, 1980 [3]. The differential equations are integrated over each volume yielding a set of algebraic equations. Internodal variation for the dependent variables can be of different kind corresponding to different *finite-difference* formulations. In the present work, for simplicity, the *Upwind Differencing Scheme* is used to model convective fluxes across volume faces. However, the formulation below is presented in such way that no difficulties arise if another differencing scheme is employed.

Discretized Equations. The block-implicit arrangement below for the flow and continuity equations, as mentioned, was first presented by Vanka [9,10]. For the sake of completeness when extending it to buoyant and swirling problems, the flow equations are here also included. Integrating then the continuity equation around point (*ij*) (see notation in Figure 1) following standard practices in numerical differentiation, one has [3]:

$$F_i^1 U_{i+1/2,j} - F_i^2 U_{i-1/2,j} + F_j^1 W_{i,j+1/2} - F_j^2 W_{i,j-1/2} = 0 \tag{2}$$

where the geometric coefficients *F*'s make computations convenient and efficient and can be interpreted as (area of flow)/(volume of computational node). For the radial momentum equation the final form for the $U_{i-1/2,j}$ component contains coefficients representing influences by convection and diffusion mechanisms in addition to all sources and pressure gradient terms. For application in the numerical algorithm below, the equation can be written in such a way that [15]:

$$U_{i-\frac{1}{2},j} = \hat{U}_{i-\frac{1}{2},j} + \hat{d}_{i-\frac{1}{2}}\left[P_{i-1,j} - P_{i,j}\right] + \hat{e}_{i-\frac{1}{2}} V_{i,j} \tag{3}$$

In (3) , *P* is the pressure and the last term on the right hand side represents the influence of *V* on the radial velocity *U* and entails a linearization of the *centripetal* acceleration [15]. All sources term, except the pressure gradient and the contribution due to the tangential velocity, are compacted in the first term on the right hand side. For the coupled treatment here presented, the explicit contribution of *V* in the source term of *U* is necessary, as it will be seen below.

A similar equation for the axial velocity component $W_{i,j-1/2}$ is given by:

$$W_{i,j-\frac{1}{2}} = \hat{W}_{i,j-\frac{1}{2}} + \hat{d}_{j-\frac{1}{2}}\left[P_{i,j-1} - P_{i,j}\right] + \hat{g}_{j-\frac{1}{2}} \Theta_{i,j} \tag{4}$$

For natural convection flows oriented as in Figure 1, the non-dimensional temperature Θ appearing in (4) is defined as $\Theta = (T-T_0)/(T_1-T_0)$ and is based on the maximum temperature drop across the computational domain $\Delta T=(T_1-T_0)$. Accordingly, here again it is important to notice that the source term in (4) explicitly shows the contribution of *T* (or Θ) on *W*. For the coupled treatment here presented, this explicit arrangement is also as shown later.

Following then a similar procedure for the Θ and *V* equations, final finite-difference equations can be assembled in the following form:

$$a_{ij}^{\Theta}\Theta_{i,j} = b_{ij}^{\Theta}\Theta_{i+1,j} + c_{ij}^{\Theta}\Theta_{i-1,j} + d_{ij}^{\Theta}\Theta_{i,j+1} + e_{ij}^{\Theta}\Theta_{i,j-1} \tag{5}$$

$$a_{ij}^{V} V_{i,j} = b_{ij}^{V} V_{i+1,j} + c_{ij}^{V} V_{i-1,j} + d_{ij}^{V} V_{i,j+1} + e_{ij}^{V} V_{i,j-1} + f_{ij}^{V} + g_{ij}^{V} U_{i,j} \tag{6}$$

It is interesting to observe that the last term in (6) comes from discretization of the *Coriollis* acceleration in the *V*-equation and represents the feedback effect of the cross-flow on the tangential velocity (see Table **1**). In this work, however, this term is not treated implicitly and, when solving for *V*, it is compacted in the explicitly-treated source term. The *centripetal* acceleration, however (see Table 1 and equation 3), is here implicitly handled. The explicit treatment is also employed when discretizing the *convection* terms in the *T* and *V* equations since no particular terms with *U's* or *W's* are shown in (5)-(6).

For simplicity, equations (5)-(6) can be rearranged such that

$$\Theta_{i,j} = \hat{\Theta}_{i,j}\,; \quad V_{i,j} = \hat{V}_{i,j} \tag{7}$$

where,

$$\hat{\Theta}_{i,j} = \left\{ b_{i,j}^{\Theta}\Theta_{i+1,j} + c_{i,j}^{\Theta}\Theta_{i-1,j} + d_{i,j}^{\Theta}\Theta_{i,j+1} + e_{i,j}^{\Theta}\Theta_{i,j-1} \right\} / a_{i,j}^{\Theta}$$

$$\hat{V}_{i,j} = \left\{ b^V_{i,j} V_{i+1,j} + c^V_{i,j} V_{i-1,j} + d^V_{i,j} V_{i,j+1} + e^V_{i,j} V_{i,j-1} + f^V_{i,j} + g^V_{i,j} U_{i,j} \right\} \Big/ a^V_{i,j} \tag{8}$$

Numerical Strategy. In order smooth out errors due to initial guessed fields, *corrections* are defined as differences between *exact* and *not-yet-converged* variables. Residuals for momentum transport at each control volume face, continuity of mass and ϕ equations are obtained by applying the just defined *approximate* values into (3)-(4)-(7). After some manipulation (details in 12,15) a system connecting the residuals and corrections can be written into matrix form as,

$$\begin{bmatrix} 1 & 0 & 0 & 0 & \hat{d}_{i-\frac{1}{2},j} & 0 & \hat{e}_{i-\frac{1}{2}} \\ 0 & 1 & 0 & 0 & -\hat{d}_{i-\frac{1}{2},j} & 0 & \hat{e}_{i-\frac{1}{2}} \\ 0 & 0 & 1 & 0 & \hat{d}_{i,j-\frac{1}{2}} & \hat{g}_{j-\frac{1}{2}} & 0 \\ 0 & 0 & 0 & 1 & -\hat{d}_{i-\frac{1}{2},j} & \hat{g}_{j+\frac{1}{2}} & 0 \\ -F^1_i & F^2_i & -F^1_j & F^2_j & 0 & 0 & 0 \\ 0 & 0 & 0 & 0 & 0 & 1 & 0 \\ 0 & 0 & 0 & 0 & 0 & 0 & 1 \end{bmatrix} \begin{bmatrix} U'_{i-\frac{1}{2},j} \\ U'_{i+\frac{1}{2},j} \\ W'_{i,j-\frac{1}{2}} \\ W'_{i,j+\frac{1}{2}} \\ P'_{i,j} \\ \Theta'_{i,j} \\ V'_{i,j} \end{bmatrix} = \begin{bmatrix} R_{i-\frac{1}{2},j} \\ R_{i+\frac{1}{2},j} \\ R_{i,j-\frac{1}{2}} \\ R_{i,j+\frac{1}{2}} \\ R_{i,j} \\ R^{\Theta}_{i,j} \\ R^{V}_{i,j} \end{bmatrix} \tag{9}$$

where the subscript identify locations in the grid, the superscript ' distinguishes corrections and the l.h.s. represents the residue vector calculated at previous iteration.

In (9) the influence of Θ on the flow field is directly accounted for by the *e*-terms. Similarly, the influence of *V* on *U* is implicitly considered by the *g*-terms. For the radial and axial directions, the *g*- and *e*-terms are of null value, respectively. As mentioned before, the reverse effect, or say the cross-flow influence on the Θ and *V* fields is here not treated implicitly. The solution of system (9) is then easily obtained by finding first corrections for Θ and *V*, calculating later the pressure *P* and velocity components *U* and *W*. Essentially, the method consists of finding the corrective values for *U*, *V* and *P*, such that the balance equations are correctly satisfied.

Boundary conditions. Boundary conditions used for all velocity components were given value at the flow inlet and non-slip condition at chamber walls. For cells facing the outlet plane, overall mass-conservation balance at each computational cell was used to calculate the control-volume outgoing axial velocity (at the top lid). Initial null values were set for all velocities.

For temperature, a linear profile along the vertical direction was assumed to prevail over the lateral wall (see Figure 1). Except in the opened areas, at the bottom and at the top, the non-dimensional temperature took the values +1 and -1, respectively. Through the inlet and outlet areas, the applied boundary conditions for the temperature were $\Theta = 0$ and $\partial\Theta/\partial z = 0$, respectively.

Numerical implementation of boundary conditions was achieved by maintaining the constant initial values at the boundaries, where applicable, or by updating them at each iteration, as in the cases of outlet surfaces or symmetry line.

All computations below used a 18x36 **single** grid equally distributed in the domain of calculation. An essential characteristic of Vanka's work, the *multigrid* artifice, has <u>not</u> been used in the present work due to the relatively modest grid here analyzed. Multigrid techniques are known to perform well with mid-size to large grids, but are rather ineffective when applied to small size problems. For this reason, no multigrid or any other large grid accelerating scheme was implemented.

Computational Parameters. The same relaxation parameters (α=0.55 for *U, W, P, V* and Θ) were used in all calculations. The swirling strength, *S*, Reynolds number, *Re*, and Rayleigh number, *Ra*, are defined as,

$$S = \left.\frac{V}{W}\right)_{in} \; ; \; \mathrm{Re} = \frac{W_{in}\, 2\, R}{\mu} \; ; \; Ra = \frac{Pr\rho^2 \beta\, g_z \Delta \mathrm{T}\, R^3}{\mu^2} \tag{10}$$

These three parameters were varied in the range $1< S <10^3$, $2< Re <10^3$ and $10^2< Ra <10^5$. The incoming axial velocity at inlet, W_{in} , was such that the Reynolds number, in most of the cases run, took the value in the range 2-200. This relatively small input value for W_{in} indicates that although the flow comes inside the chamber with appreciable rotation (S up to 10^3), it carries almost no momentum in the axial direction. This incoming velocity level was found to be consistent with the weak currents driven in a thermally-driven flow. With that, cases with balanced *natural* and *forced* convection mechanisms could be analyzed.

Partially Segregated Scheme. The algebraic equations for the velocity field were solved, in addition to the fully-coupled scheme here described, by performing outer iterations for the components Θ and V while keeping U-W-P from the previous iteration. A *line-by-line* smoothing operator, fully described elsewhere (e.g. [3]), was used to relax Θ and V, being the secondary flow field (U,W) calculated by the locally-coupled method seen above. This *partially segregated* solution was set in such a way that the same number of sweeps throughout the scalar (Θ,V) and cross-flow fields (U,W,P) was obtained. Since in the coupled scheme every sweep for U-W-P also implies in smoothing out Θ-V errors, this procedure was found to be a reasonable way to fairly compare the two methods. In all partially segregated computations, a total of four sweeps per scalar per outer iteration was performed.

The reason for recalling this second procedure a *partial* rather than a *full* segregated scheme lies in the fact that in full segregated methods all variables, including U, W and P, are solved independently and in sequence along the entire algorithm. In the case here presented for comparison, only Θ and V are excluded from the implicit treatment implied by eqn. (9).

3. RESULTS AND DISCUSSION

Temperature Field. Figure 2 shows results for the temperature field when subjected to an increase in the incoming mass flow rate (increase in Re, see eqn. 10). The Figure indicates that the core of the flow becomes homogenized as more fluid comes into the chamber due to higher recirculating motion in the r-z plane. Outlet temperatures are correctly increased when the higher axial mass flow rate sweeps hot fluid from bottom layers through the exit (see Figure 1 for geometry details). Increase of the central recirculating bubble is also clearly detected by the downward wash of isolines at the centerline.

Figure 3 shows calculations for the temperature field done with different values for Ra spanning from 10^2 to 10^4. Distortion of the temperature profiles also indicates strength of convective ascending currents close to the wall with corresponding downward motion at the central region. Interesting to note is the increase in temperature gradients close to the center, at the bottom lid, due to the just mentioned downward stream. When analyzing real equipment, not subjected to the imposed b.c.'s here used, steep gradients of temperature close to walls might be an indication of possible temperature raise at some particular locations. Design engineers may then use this sort of information to overcome potential material damage when performing preliminary thermal design.

Figure 4 presents the temperature pattern for different values of S. Interesting to note is the small effect on T, even though S changes by such a large factor of 10^3. Considering the assumed axi-symmetry of the flow, a strong rotation will carry fluid tangentially, essentially through zones of equal temperature. On the other hand, an increase in Re or Ra, shown in Figures 2 and 3, substantially distort the temperature by increasing the ascending cross-flow currents. One should mention that in a real fully three-dimensional flows in industrial equipment ascending currents are quite strong, playing certainly a definite role in establishing the temperature pattern inside such domains. For the simplified flow and geometry here analyzed, however, no such effect was expected.

Residue History. Normalized residues were defined as the norm of the cell residue for mass, energy and tangential velocity equations as,

$$R_{abs} = \left\{ \sum_{i\,j} \left(R_{ij}\right)^2 \Big/ (N \cdot M) \right\}^{\frac{1}{2}} \qquad \textbf{(11)}$$

where ϕ in (11) refers to the general transport variable as defined in Table 1, N and M are the number of cells in the *r*- and *z*-directions, respectively. For continuity equation, R_{ij} can be seen as the difference, for every cell, between the cell outgoing mass flux, F_{out}, and the incoming mass flux, F_{in}. A *relative* mass residue can then be defined as,

$$R_{rel} = \left\{ \sum_{i\,j} \left(\frac{F_{out} - F_{in}}{F_{out} + F_{in}} \right)^2 \Big/ (N \cdot M) \right\}^{\frac{1}{2}} \qquad \textbf{(12)}$$

A discussion on the advantages in simultaneously monitoring R_{rel} in addition to R_{abs} is presented in de Lemos 1990, 1992 [11,12] and it is based on the small range of the former (0,+1).

The three parameters here investigated, namely *Re*, *Ra* and *S*, were analyzed in terms of their influence on the overall convergence rates. Results are shown in Figures 5, 6 and 7, respectively. The iteration counter refers to the total number of sweeps over the domain, that is, the product of the outer counter times the number of inner sweeps. Here, a quick word on the numbers of iterations to convergence seems timely. Other schemes presented in the literature may indicate residue history as a function of outer iteration counters only. Some, use the so-called pseudo-transient approach and plot time steps instead. Each outer iteration, in turn, may consider a great number of internal sweeps, usually controlled by a specified residue reduction rate. Here, in this work, a fixed number of internal sweeps was considered. The relatively large number of necessary iterations seen in the figures below could be associated with the use of a single grid, the tightness of the relaxation parameters and the strong coupling among all variables involved.

Interesting to note is the better convergence performance for the higher Reynolds number (see Figure 5), possibly reflecting the fact that, as *Re* increases, the flow becomes more *forced-convection* dominated decreasing the *UW-T* coupling in relation to the *UW-P* connection. This, in turn, facilitates the solution of the energy equation once the velocity field is calculated. This idea is supported when Figure 6 is inspected, showing worse convergence rates for a higher *Ra*. There, the higher degree of coupling between temperature and cross-flow fields makes computation more demanding, reflecting the increase in physical coupling among the flow variables and temperature.

On the other hand, when *S* is varied, Figure 7 shows a weak dependency of R_T on the swirling strength. According to Figure 4, no substantial change on temperature patterns was detected when inlet rotation increases (except for S=10^3). For such small inlet mass flow rates (*Re*=2), viscous shear driven by the incoming swirling motion enhances the cross-flow field which, in turn, distorts isothermal lines. Such an indirect or second-order relationship between V and $\boldsymbol{T}$ is apparently also reflected on the residue histories shown in Figure 7.

Finally, the Figures seems to indicate also that the cross-flow field can quickly adjust itself to changes in the scalar profiles, and that, in the segregated case, those changes are too slowly transferred back to Θ-V. The coupled solution, however, quickly transmits back to Θ *and V*-equations changes in the cross-flow pattern, more realistic simulating the strong interaction among the variables involved.

4. CONCLUDING REMARKS

This paper detailed a fully-coupled technique for numerical prediction of ascending heated swirling flows in a cylindrical chamber. An extension of the numerical method in Vanka, 1986 [9,10] towards a fully implicit solution of the energy, tangential and cross-flow equations was reported. Outlining of the numerical method showed the necessary steps for setting up the residuals and the methodology used to calculate the corrections for all dependent variables. Comparison of partially-segregated and fully-coupled treatments for the energy and tangential velocity shows a lower computer effort when the latter method was used. The approach herein is promising regarding numerical stability of the entire equation set since inherent coupling among the variables is implicitly handled. Further, it is also expected that more advanced computer architectures can benefit from the point wise error smoothing operator here described.

5. ACKNOWLEDGMENTS

The author is thakfull to CNPq, Brazil, for their financial support during the preparation of this work.

6. REFERENCES

1. de Vahl Davis, G. Natural Convention Of Air In A Square Cavity: a Bench Mark Numerical Solution, *Int. J. Num. Meth. Fluids*, vol. 3, pp. 249-264, 1983.
2. M. Hortmann, M. Periç and G. Scheider, Finite Volume Multigrid Predictions of Laminar Natural Convection: Benchmark solutions, *Int. J. Num. Meth. Fluids*, vol. 11, pp. 189-207, 1990.
3. Patankar, SV. *Numerical Heat Transfer and Fluid Flow*, Mc-Graw Hill:New York, 1980.
4. P. F. Galpin and G. D. Raithby, Numerical Solution of Problems in Incompressible Flow: Temperature of the temperature Velocity Coupling, *Num. Heat Transfer* 1986, **9**(1):105-129.
5. L. Tang and Y. K. Joshi, Application of Block Implicit Multigrid Approach to Three-dimensional Heat transfer Problems Involving Discrete Heating, *Num. Heat Transfer – Prt. A*, vol. 35, pp. 717-734, 1999.
6. Hogg, S., Leschiziner, MA. Second-moment-closure calculation of strongly swirling confined flow wit large density gradients, *Int. J. Heat and Fluid Flow* 1989, **10**(1):16-27.
7. Hogg, S., Leschiziner, MA. Computation of Highly Swirling Confined Flow with as Reynolds Stress Turbulence Model, *AIAA J.* 1989, **27**(1):57-63.
8. Nikjook, M., Mongia, HC. A second-order modeling study of confined swirling flows, , *Int. J. Heat and Fluid Flow* 1991, **12**(1):12-19.
9. Vanka SP. A Calculation Procedure for Three-Dimensional Steady Recirculating Flows Using Multigrid Methods, *Comp. Meth. App. Mech. Eng.* 1986, **55**:321-338.
10. Vanka SP. Block- Implicit Multigrid Solution of Navier- Stokes Equations in Primitive Variables, *J. Comp. Phys* 1986, **65**:138-158.
11. de Lemos, MJS. Computation of Laminar Axi-Symmetric Recirculating Flows Using Primitive Variables and a Block-Implicit Scheme, *Proc. of ENCIT90 - 3rd Braz. Therm. Sci. Meeting* 1990, **1**:375-380, Itapema, SC, Brazil, December 10-12.
12. de Lemos, MJS. Computation of Buoyancy-Driven Flows Using a Block-Implicit Numerical Scheme, *Proc. of the 28th Nat. Heat Transfer Conf.* 1992, HTD-**194**:83-89, San Diego, CA, USA, August 9-12.
13. de Lemos, MJS. Locally-Coupled Numerical Solution of Thermally-Driven Cavity Flows, *Proc. of COBEM97- 14th Braz. Congr. Mech. Eng.* 1997, Bauru, SP, Brazil, December 8-12.
14. de Lemos, MJS. Cell-Implicit Numerical Computation of Flow Field And Heat Transfer in Inclined Cavities, *Proc. of COBEM97-14th Braz. Congr. Mech. Eng.* 1997 (in CD-ROM), Bauru, SP, Brazil, December 8-12.
15. de Lemos, MJS. Simulation of Swirling Flow in A Model Combustor Using A Locally-Coupled Numerical Method, *Proc. of Winter Annual Meeting of the ASME* 1992, HTD-**226:**79-84, Anaheim, CA, USA, November 8-13

Table 1 - Terms in the general transport

	ϕ	Γ_ϕ	S_ϕ
Continuity	1	0	0
Axial Momentum	W	μ	$-\frac{\partial P}{\partial z} + \rho_0 g_z \beta \left(T - T_0\right)$
Radial Momentum	U	μ	$-\left(\frac{\partial P}{\partial r} + \frac{\mu U}{r^2} - \frac{\rho \mu V^2}{r}\right)$
Azimuthal Momentum	V	μ	$-\left(\frac{\mu V}{r^2} + \frac{\rho U V}{r}\right)$
Energy	T	μ / Pr	0

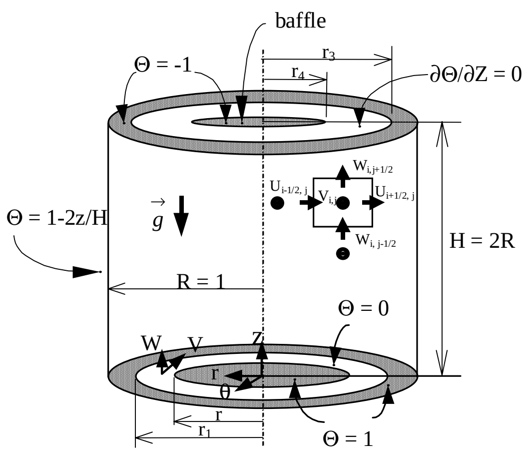

Figure 1 - Vertical cylindrical chamber

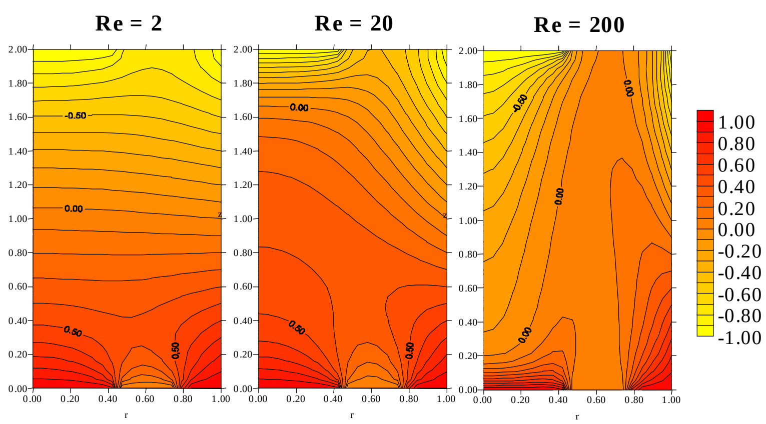

Figure 2 - Effect of *Re* on temperature field, S=1, Ra=10^2.

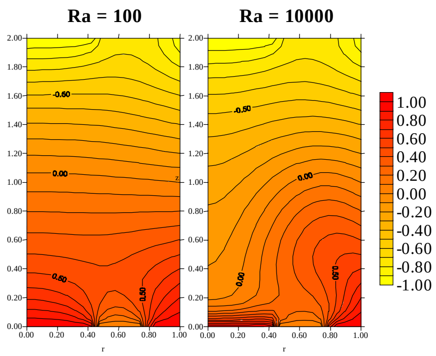

Figure 3 - Effect of *Ra* on temperature field, *Re*=2, *S*=1.

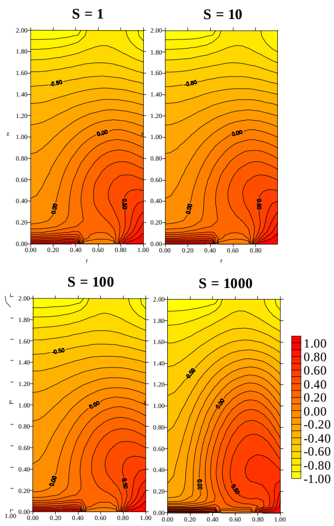

Figure 4 – Effect of swirling strength on temperature, $Ra=10^4$, $Re=2$.

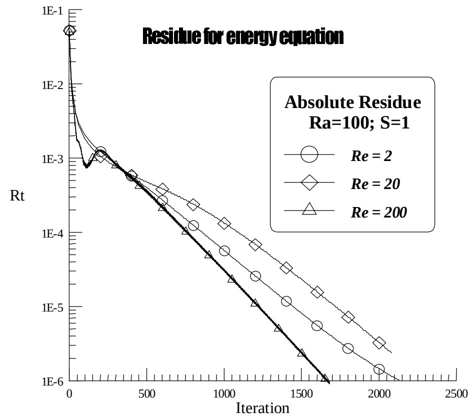

Figure 5 - Influence of *Re* on convergence rate of *T*-equation**.**

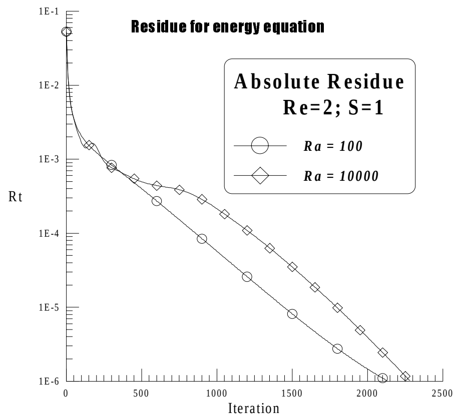

Figure 6 – Effect of *Ra* on R_T

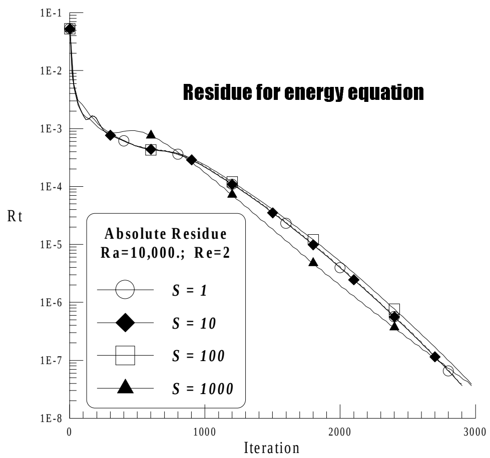

Figure 7 – Effect of swirling strength *S* on R_T.